Determinants of Microvascular Network Topologies in Implanted Neovasculatures

Carlos C. Chang, Laxminarayanan Krishnan, Sara S. Nunes, Kenneth H. Church, Lowell T. Edgar, Eugene D. Boland, Jeffery A. Weiss, Stuart K. Williams, James B. Hoying

Objective—During neovascularization, the end result is a new functional microcirculation composed of a network of mature microvessels with specific topologies. Although much is known concerning the mechanisms underlying the initiation of angiogenesis, it remains unclear how the final architecture of microcirculatory beds is regulated. To begin to address this, we determined the impact of angiogenic neovessel prepatterning on the final microvascular network topology using a model of implant neovascularization.

Methods and Results—We used 3D direct-write bioprinting or physical constraints in a manner permitting postangiogenesis vascular remodeling and adaptation to pattern angiogenic microvascular precursors (neovessels formed from isolated microvessel segments) in 3D collagen gels before implantation and subsequent network formation. Neovasculatures prepatterned into parallel arrays formed functional networks after 4 weeks postimplantation but lost the prepatterned architecture. However, maintenance of uniaxial physical constraints during postangiogenesis remodeling of the implanted neovasculatures produced networks with aligned microvessels, as well as an altered proportional distribution of arterioles, capillaries, and venules.

Conclusion—Here we show that network topology resulting from implanted microvessel precursors is independent from prepatterning of precursors but can be influenced by a patterning stimulus involving tissue deformation during postangiogenesis remodeling and maturation. **(*Arterioscler Thromb Vasc Biol*. 2012;32:5-14.)**

Key Words: angiogenesis ■ microcirculation ■ morphogenesis ■ vascular biology

In the therapeutic repair or reconstruction of the microvasculature, it is important to consider that the goal is to form a new functional microcirculation. Thus, a successful therapeutic outcome critically depends on not only the presence of new vessels (eg, due to angiogenesis) but also the progression of these new vessels into a microvascular network with a topology that appropriately meets tissue perfusion and functional demands.[1,2] In the native tissue, this topology typically involves a hierarchical tree organized to reflect the architecture specific to the target tissue.[3] Although we have insight into the stimuli and processes underlying microvessel diameter adaptation,[4–9] we know little concerning the determinants of microvessel spatial organization within a network. Possible relevant factors may include the influence of preexisting angioarchitectures from which the new segments are generated; guided/directed angiogenesis; the processes of network revision, including pruning; and tissue microenvironment features, including stroma architecture and tissue biomechanics. Presumably, 1 or more of these and potentially other processes interplay to control the spatial organization of the new microvessel segments as the new microcirculation evolves. To begin addressing this issue, we tested the hypothesis that the preexisting spatial organization of neovessel segments dictates the topology of the developing microvascular network.

We have previously reported that neovasculatures composed of isolated, intact microvessel segments (arterioles, capillaries, and venules) suspended in collagen type I gels (called a microvascular construct [MVC])[10] spontaneously undergo sprouting angiogenesis in culture and form functional, hierarchical microvascular networks when implanted.[4,11–13] In this system, a mature microcirculation forms from neovessels generated via angiogenic sprouting that progress into an immature network and subsequently mature via structural adaptation and network remodeling into a microcirculation.[4,13] The transition from angiogenesis to postangiogenesis remodeling coincides with the initiation of blood perfusion through the newly formed vessels with postangiogenesis

Received on: September 13, 2011; final version accepted on: October 24, 2011.

From the Cardiovascular Innovation Institute, Jewish Hospital/St. Mary's Healthcare and University of Louisville, Louisville KY (C.C.C., L.K., S.S.N., E.D.B., S.K.W., J.B.H.); nScrypt, Inc., Orlando, FL (K.H.C.); Department of Bioengineering and Scientific Computing and Imaging Institute, University of Utah, Salt Lake City, UT (L.T.E., J.A.W.).

Drs Chang and Krishnan contributed equally to this work.

Correspondence to James B. Hoying, PhD, Division of Cardiovascular Therapeutics, Cardiovascular Innovation Institute, 302 E Muhammad Ali Blvd, Louisville, KY 40202. E-mail jay.hoying@louisville.edu

Arterioscler Thromb Vasc Biol **is available at http://atvb.ahajournals.org** **DOI: 10.1161/ATVBAHA.111.238725**

processes continuing for 3 or more weeks as individual vessel segments mature and network topologies revise.[4] Of particular relevance is that more than 90% of the microvessels making up the final, mature network in the implanted MVC are derived from the initial isolate used to form the MVC.[13]

We have previously used these MVCs in a number of applications to prevent the progression of ischemic lesions following myocardial infarction,[12] to improve biomaterial biocompatibility,[11] to support islet transplantation,[14] and to generate prevascularized tissue constructs.[15,16] Furthermore, we have developed an in vitro culture system that supports scale-up of the MVCs and MVC engineering.[17] In all of these applications, the MVCs were composed of randomly oriented (ie, nonpatterned) neovessels that spontaneously generated mature microcirculations with random (ie, not predefined) network topologies. Here, we used the MVC system to determine whether or not the initial organization or arrangement of isolated neovessels in the MVC dictates the topology of the resultant microvessel network following implantation.

Methods

All animal studies were performed with protocols approved by the University of Louisville institutional animal care and use committee and according to the National Institutes of Health *Guidelines for the Care and Use of Laboratory Animals*.

MVC

To make the MVC, rat fat microvessel fragments (RFMFs) were isolated as previously described[4] from epididymal fat pads of male green fluorescent protein–expressing transgenic Sprague Dawley rats[18] and suspended in ice-cold, pH-neutral 3 mg/mL collagen type I (BD Biosciences, Sparks, MD) in Dulbecco's modified Eagle's medium (Invitrogen, Carlsbad, CA). RFMF densities used were as follows: 80,000 RFMF/mL for bioprinting, 40,000 RFMF/mL for framing, and 20,000 RFMF/mL for unframing. MVCs were cultured in Dulbecco's modified Eagle's medium containing 10% FBS. When implanted, MVCs were placed into subcutaneous pockets on the flanks of immunocompromised mice (*Rag1* null bred 10 generations onto the C57BL/6J, Jackson Laboratory) as previously described.[4]

Electrospinning

Fraction I bovine fibrinogen (MP Biomedicals, Solon, OH) was dissolved at a concentration of 100 mg/mL in 90% 1,1,1,3,3,3-hexafluoro-2-propanol (Sigma-Aldrich) in minimal essential medium (Lonza, Allendale, NJ). The fibrinogen solution was dispensed via syringe pump (1.5 mL/h) at +20 to +25 kV DC toward an oscillating stainless steel mandrel rotating between 1000 and 5000 rpm to form a thin mat.[19]

Bioprinting

Printed MVCs were prepared using the BioAssembly Tool (BAT).[20] The BAT is composed of a computer-controlled stage, which permits independent x and y translation with 500 nm resolution, and a z translational print head independently controlled with the same resolution. The system is currently configured with 2 independently controlled dispensing systems, a servo-controlled displacement pump and a pneumatic-controlled air syringe (Supplemental Figure I, available online at http://atvb.ahajournals.org). The former is typically used to dispense low-viscosity materials (such as 3 mg/mL collagen), and the latter is used for higher viscosity materials (such as 40% wt/vol Pluronic F127). Each syringe cartridge contains copper coils that are plumbed to separate temperature-controlled circulators. In this manner, we are able to maintain precise control of sample temperature while bioprinting. While printing, 1 syringe is lowered to the printing surface. Cameras attached to the syringe cartridge permit real-time monitoring of the printed structures. Either syringe may be lowered to the printing surface at any time during the printing run. Calibration between syringes permits $x/y/z$ accuracy of ± 10 μm and x/y precision of ± 2 μm.

Bioprinting designs were first scripted (see Supplemental Data), then compiled by Machine Tool software (nScrypt, Orlando, FL), and then uploaded to the customized BAT.[21] Separate, sterile 5 mL syringes equipped with low-viscosity pistons (Nordson EFD, Westlake, OH) were aseptically filled with either RFMF-collagen or sterile 40% (wt/vol) Pluronic F127 (Sigma Aldrich) in PBS. Syringes were then inserted into the precooled displacement pen (RFMF-collagen) and the room-temperature air syringe (F127) of the BAT. Multiple MVCs were printed onto a single electrospun fibrinogen mat by first dispensing F127-PBS followed immediately by dispensing RFMF-collagen into the formed channels (see Supplemental Movie I; printing parameters described in Supplemental Table I). Following polymerization of the collagen at 37°C, the F127 was rinsed away with cold saline, and individual printed MVCs were then cut from the larger sheet and then cultured or implanted.

Framing MVCs

For the unframed implants, small pieces of 316L SS stainless steel mesh (Small Parts) were attached to opposite walls of a Laboratory-Tek II slide chamber (Nunc) with Loctite UV glue (Henkel, Düsseldorf, Germany). For framed implants, the mesh was bent into an elongated U shape with the long bottom of the U coated in UV glue to prevent collagen attachment. The U frame maintained tension across the MVC during implantation. In both cases, collagen enveloped the mesh ends forming a robust attachment. Teflon blocks were placed on either side of the mesh in the chamber to form a rectangular space with mesh pieces making up each end. RFMF-collagen ($\approx$1.0 mL) was pipetted into the space and polymerized, and the Teflon blocks were removed.

Morphometry

After 1 or 4 weeks, perfusion through implants was assessed by injecting host mice with either 200 μL of rhodamine-conjugated 2,000,000 molecular weight dextran (Invitrogen) or GS-1 lectin conjugated to rhodamine (Vector Laboratories, Burlingame, CA) into the jugular vein.[4] After 15 minutes, implants were harvested and fixed overnight in 2% paraformaldehyde (EMD Chemicals, Gibbstown, NJ) at 4°C. For vessel morphology assessment, 2 random vascularized areas per unframed construct and 3 areas from the framed constructs (2 ends and middle) were imaged with an Olympus FV1000 MPE confocal microscope. Image stacks were z-projected and binarized with ImageJ software before volume rendering before morphometry. Numbers of green fluorescent protein–positive segments and diameters (center of each vessel segment) were measured by hand. To identify perivascular cells, MVCs were incubated overnight at 4°C with an α-smooth muscle actin antibody directly conjugated to Alexa 634 as previously described.[4] The vessels were classified as arterioles if they had a robust, "banded" pattern of α-actin coverage; as venules if they had lesser and nonarteriolar pattern of smooth muscle coverage; and as capillaries if they did not fit into these 2 groups.

Thus, each counted vessel had an associated type designation, diameter, and perfusion status expressed as a percentage of the total for the respective samples. All image volumes were first normalized to the smallest volume in both treatment groups, and this scaled relative volume was further used to normalize the observed vessel counts to account for the influence of different imaging volumes on the number of vessel segments evaluated.

Fast Fourier Transform Analysis

To quantify orientation of vessel segments, a mean intercept length approach[22] was used using a custom MATLAB script and Fourier-transformed images. The magnitude and direction of the principle mean intercept length axes of the vessel segments was then used to determine an "anisotropy index" α:

$$\alpha = 1 - \lambda_1/\lambda_2$$

where $\lambda_1 < \lambda_2$, and λ_1 and λ_2 are the eigenvalues describing the minor and major axes, respectively, of the fit mean intercept length ellipse. The anisotropy index was used as a measure of the alignment, such that $\alpha=0$ indicates random orientation and $\alpha=1$ indicates perfect alignment in a principal direction.

Statistical Analysis

The anisotropy indices of the 4 groups were compared using Kruskal-Wallis 1-way ANOVA on ranks (unequal variance) followed by post hoc multiple pair-wise comparisons (the Dunn method), with $\alpha=0.05$. One-way ANOVA or its nonparametric equivalent (Kruskal-Wallis ANOVA on ranks) followed by a post hoc comparison (Tukey) was used to identify significant differences in number of vessels of each phenotype and their perfusion status (significance set at $\alpha=0.05$).

Computer Simulations

For the MVC, a rectilinear domain (20.5×6.5×3 mm) was fit with a regular hexahedral mesh with nodal spacing of 0.5 mm. A compressible neo-Hookean hyperelastic constitutive model was used to model the collagen gel (E=40 kPa, $\nu=0.0$). An active contractile force based on a uniform continuous fiber distribution was used to simulate contraction of the matrix by growing microvessel fragments.[23] The faces of the gel normal to the long axis (x-axis) were constrained to represent the boundary condition created by the stainless steel frame.

Nonlinear finite element simulations were run using FEBIO custom software. The active contractile stress was discretized over arbitrary quasi-time ($0 \le t \le 1.5$), and an incremental-iterative nonlinear solution strategy was used.[24] For the simulations, 2 finite element models were created. The first model simulated gels that remained within the stainless steel frame for the entire culture period (framed implants). The second model represented gels that were cut from the frame before implantation (cut implants). In this model, the boundary constraints were in place for the initial third of the simulation ($t=0.0$ to $t=0.5$). These constraints were removed for the remaining two thirds of the simulation ($t=0.5$ to $t=1.5$), representing the growth period after the gel had been cut away from the frame. A viscoelastic component had to be added to the constitutive model to dissipate elastic stress and prevent recoil after the constraints had been removed, as significant recoil was not observed in implants removed from their frame before implantation. The relaxation function, $G(t)$, used to dissipate elastic stress is given by the following:

$$G(t) = \gamma e^{-\frac{t}{\tau}}$$

where γ is a scaling factor and τ is the time constant and governs the rate of stress relaxation. A time constant of $\tau=2$ was used to relax a portion of elastic stress built up within the gel.

To demonstrate how deformation of the gel impacts microvessel orientation, skeletonized data of random microvessels were placed within the finite element models at the center of the initial geometry. The position of the vessel segments after the deformation was obtained by interpolating nodal displacements at the vessels' positions using trilinear shape functions:

$$v_{\text{final}} = v_{\text{initial}} + \sum_{i=1}^{8} N_i(\xi) u_i$$

In this equation, v_{initial} is the position of a vessel segment in the initial configuration, and v_{final} is the position of a vessel segment in the deformed configuration. N_i is the shape function for node i of the element in which the vessel resides, and ξ is the position of the vessel segment in that element's natural reference frame.

Results

We used 2 different approaches to generate MVCs with aligned neovessels, both of which permitted patterned neovessels to undergo postangiogenesis neovessel remodeling, including vessel type specification and structural adaptation. The first neovessel prepatterning strategy exploited the rheological phenomena associated with the narrowed extrusion of relatively rigid fibers in a liquid suspension[25] to uniaxially align isolated microvessels in unpolymerized collagen. To do this, we used a direct-write, 3D bioprinting tool (BAT) equipped with independently operated, temperature

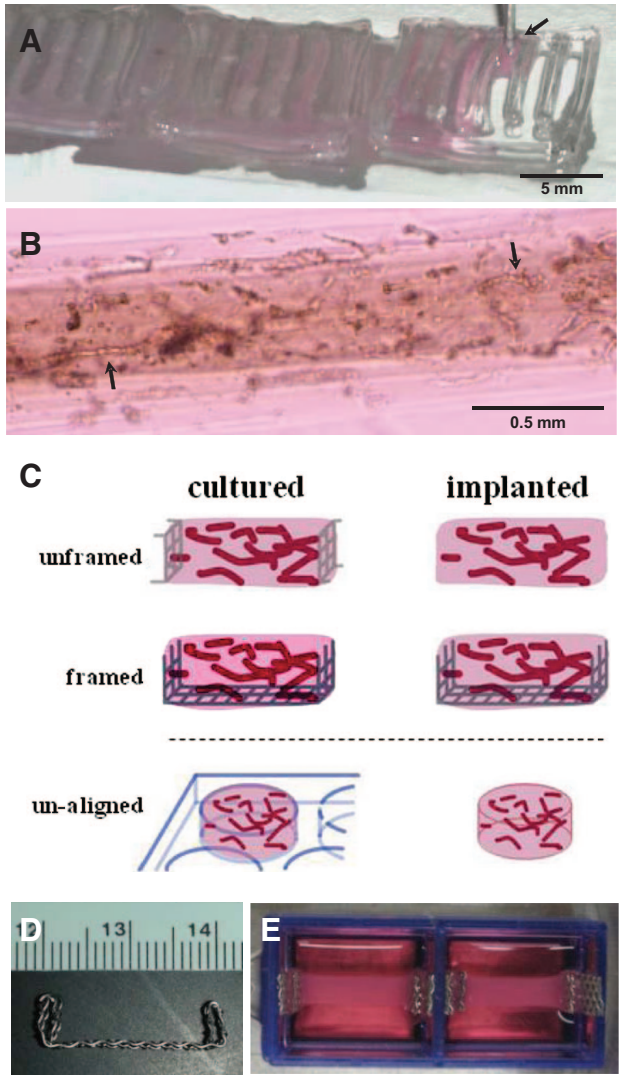

Figure 1. Microvascular constructs (MVCs) formed by 3D printing using the BioAssembly Tool or by physical framing. **A**, Still image of the final fill stage from a video clip (see Supplemental Movie I) of MVC printing showing the printing tip (arrow) dispensing collagen fragments in the hydrogel mold. **B**, A phase image of a newly bioprinted MVC with microvessel fragments (arrows) dispersed throughout the stripe of collagen. **C**, Schematic of the different constrained conditions. MVCs constructs were placed in a frame that constrained along the single long axis. Following culture, the construct was either removed from the frame ("unframed") or kept in the frame ("framed") for implantation. Unaligned MVCs were prepared by forming the constructs in well plates, which constrain radially, and removing them before implantation. **D**, Side view of the stainless steel frame used in the framed experiments, made from screen cut in long strips and then folded in at the ends to allow for better construct anchoring. Scale is in centimeters. **E**, Top view of framed MVCs in culture used for unframed implants.

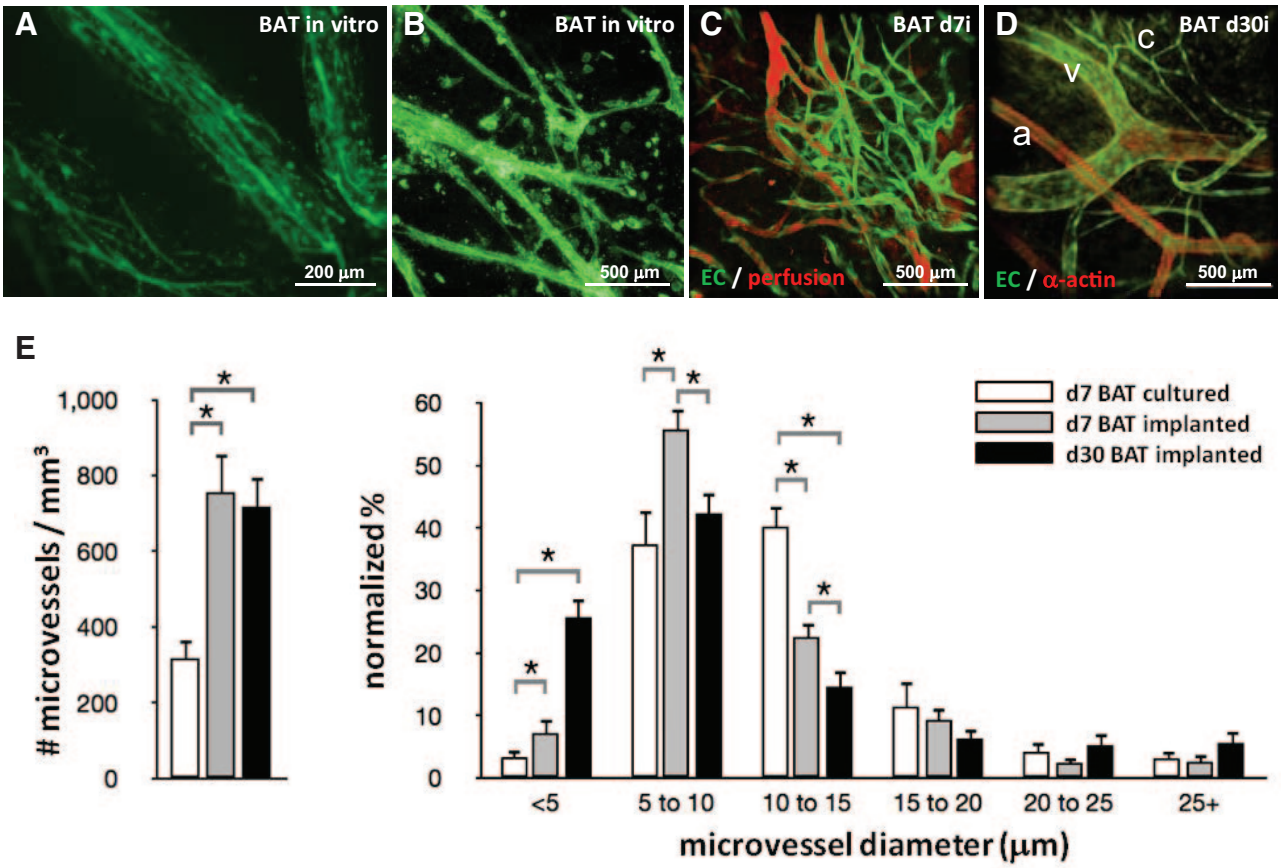

Figure 2. Microvascular networks formed in implanted microvascular constructs (MVCs) did not maintain a prealigned orientation. **A** and **B**, Low-magnification epifluorescence image (**A**) and high-magnification confocal stack (**B**) of angiogenic neovessels formed from isolated parent microvessel fragments (isolated from green fluorescent protein–expressing transgenic rats) in BioAssembly Tool (BAT)–printed MVCs cultured for 7 days. **C**, Following implantation, the neovessels within the BAT-printed MVC lines assembled into a simple network and were perfused after 7 days postimplantation (BAT d7i). **D**, After 30 days postimplantation (BAT d30i), mature arterioles (a), capillaries (c), and venules (v) were present within a hierarchical network. **E**, The density of microvessels and the percentage distribution of microvessels of a given diameter in printed MVCs. All values are presented as mean±standard error of the mean. Statistical significance was determined using 1-way ANOVA with post hoc comparison ($P \leq 0.05$ was considered significant). Legend applies to both data graphs. EC indicates endothelial cell.

controlled syringes capable of dispensing as little as 20 pL of fluids deposited at 100 nm resolution.[20,21,26] Because printed lines of unpolymerized collagen (3 mg/mL) with or without cells collapse and spread, we first printed dissolvable hydrogel walls to form sets of parallel channels, within which we printed unpolymerized MVCs in a second printing pass (Figure 1). To facilitate handling and later implantation, the hydrogel molded MVCs were printed onto electrospun fibrinogen mats.[19] Dispensing the isolated microvessel/collagen suspension into the hydrogel channels resulted in individual microvessel segments being oriented along the long axis of the print lines, which, following collagen polymerization and removal of the hydrogel walls, produced strips of MVCs with aligned microvessel segments (Figure 1). The second approach to prepattern neovessels was based on our previous work showing that the defined physical constraining of MVCs influences angiogenic neovessel orientation.[27–30] Using a wire frame, we physically constrained the MVC along 1 axis by maintaining opposing attachment points for the gels (Figure 1). As we have shown before, this creates a uniaxial constraint between the 2 anchors (secondary to collagen gel contraction by cell constituents) and promotes neovessel orientation parallel to the axis of attachments without significant effects on neovessel growth or morphology.[29]

After 7 days in culture, BAT-printed MVCs contained numerous neovessels, which arose from the parent microvessel segments, bounded within the printed collagen strips (Figure 2). By 7 days postimplantation, the neovessels in the BAT-printed MVC had formed a perfused yet immature network that progressed to form a perfused hierarchical network of mature microvessels with heterogeneous diameter distributions by 30 days postimplantation (Figure 2). In culture, the sprouted, angiogenic neovessels in MVCs prepared by BAT-based printing were aligned along a single, primary axis as determined by Fast Fourier transform analysis (Figure 3). However, unlike in culture, the resulting networks that formed after 30 days postimplantation exhibited low anisotropy indices matching those of randomly oriented MVC implants (Figure 3). A similar loss of anisotropy was observed with MVCs prepared by framing during the culture period followed by implantation without the frame (Figure 3). From these observations, we conclude that the spatial orientation of microvascular precursors at the time a tissue construct is assembled does

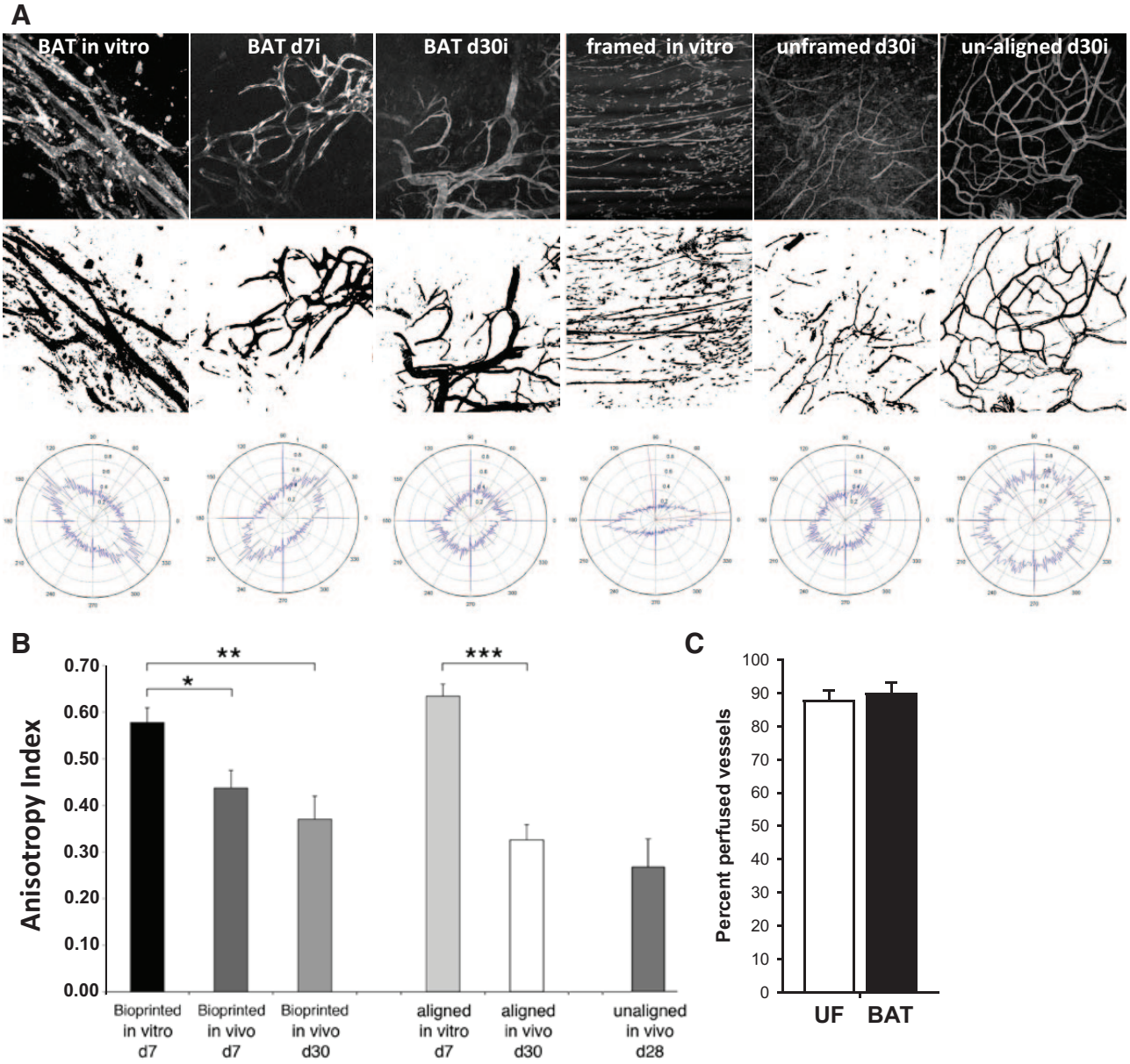

Figure 3. Fast Fourier transform (FFT)–based analysis of microvessel anisotropy in patterned microvascular constructs (MVCs). **A**, In the top row are examples of vascular fields from cultured (in vitro) and day 7 (d7i) or day 30 (d30i) implanted MVCs used in the analysis. The middle row contains the corresponding thresholded and binarized images used to generate the orientation plots by FFT (bottom row). **B**, Plot of anisotropy indices generated from the FFT analysis for each of the conditions. *$P<0.05$, **$P<0.01$, ***$P<0.001$. **C**, Percentage of vessels within unframed (UF) and bioprinted (BioAssembly Tool [BAT]) MVC implants (day 30) perfused with a fluorescent blood tracer (rhodamine-dextran, 2 million molecular weight).

not significantly influence the final topology of the microcirculatory network.

In performing the above-described experiments, we purposely removed the frame used to mechanically constrain MVCs (unframed implants) in culture before implantation, thereby removing the initial aligning stimulus during postimplantation remodeling. Reasoning that a persistent physical constraint would possibly maintain microvessel alignment during implantation, we next implanted the cultured, framed MVCs with the frame still in place (framed implants). Following 30 days of implantation, the entire MVC+frame was incorporated into a vascularized, loose connective capsule (Figure 4). However, in contrast to the unframed implants, the microvascular networks of the framed implants contained highly aligned microvessels throughout much of the implant (Figure 4).

In an effort to determine the basis for microvessel alignment in the framed implants (and, conversely, loss of alignment in the unframed implants), we performed computer simulations of construct mechanical behavior in both conditions. Modeling the collagen gel as a compressible neo-Hookean hyperelastic constitutive model and including a viscoelastic component to account for known dissipative elastic stress,[29] the simulations predicted differences in gel

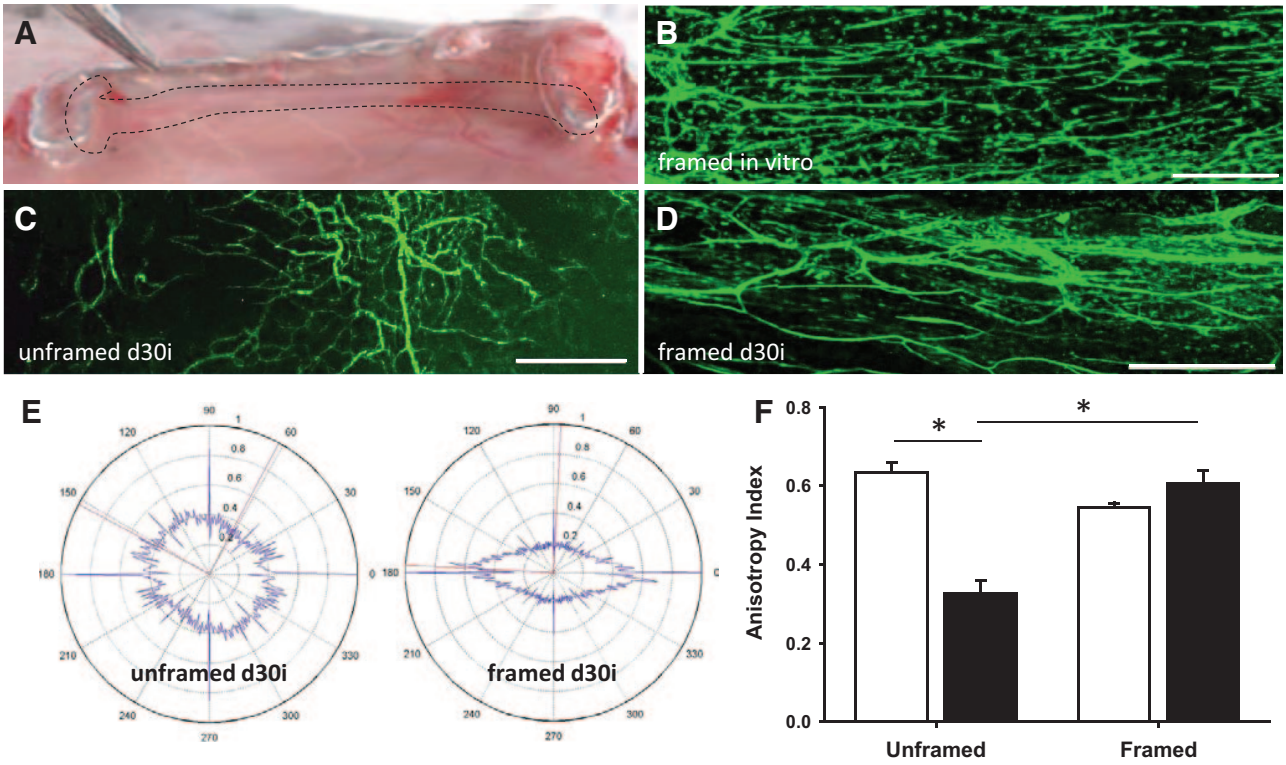

Figure 4. Microvascular construct (MVC) implants with continuous mechanical constraints formed aligned microvascular networks. **A**, Brightfield image of a framed MVC (dashed outline) explanted after 30 days of subcutaneous implantation. **B** to **D**, Stitched confocal projections showing the overall organization of the microvessels in framed cultured MVC (framed in vitro), unframed implants (unframed d30i), and framed implants (framed d30i) prepared from green fluorescent protein–expressing transgenic rats. **E** and **F**, Example FFT plots and anisotropy values for unframed and framed 30 day implants (both framed in culture) showing that continuous framing of the implants maintained microvessel alignment, whereas unframing did not. Open bars indicate cultured; filled bars, implanted.

deformation secondary to cell-based contraction. In the unframed condition, the gel deformed equally in all directions, whereas in the framed gels, contraction-dependent deformation occurred primarily transverse to the axis of constraint (Figure 5). Because of the viscoelastic nature of the collagen gel, stresses were negligible (because of a time-dependent dissipation), and strains were fairly uniform and low in the framed implants (Figure 5). The simulations predicted microvessel alignment outcomes similar to that observed experimentally (Figure 5).

Although networks in both unframed and framed MVC implants were perfused and contained all microvessel types (ie, arterioles, capillaries, and venules) intrinsic to a mature microcirculation (Figure 6), it appeared that those in the framed implants contained a higher proportion of capillaries. A morphometric analysis of the fractional composition of microvessel types confirmed that aligned networks were indeed enriched in capillaries (Figure 6). Although microvessel densities were similar between the unframed and framed implanted MVCs, framed networks had nearly half the proportion of arterioles than that in the unframed implants, whereas the fraction of venules between the 2 network systems was similar (Figure 6). The difference in the fractional distribution of microvessel types (fewer arterioles and more capillaries) in the networks of the framed implants suggests higher vascular resistance. However, mean vascular diameter was greater in these networks (Figure 6) (primarily because of significantly larger arterioles and venules). Also, there appeared to be no selective perfusion "dropout" as nearly the entire network for both unframed and framed implants was equally perfused (Figure 6). All of this suggests that blood volume flow through the aligned networks is likely comparable to, or at the least not significantly lower than, that in the nonaligned networks. That these differences are due solely to possible unique stresses and strains in the implants is unlikely. Mechanical loading of angiogenic constructs in vitro did not influence neovessel phenotype or diameter.[29] Also, the specialized parallel architecture of capillary bundles in skeletal muscle (Figure 6), similar to the architecture in the framed implants, can influence hemodynamics differently than in a pure series network of microvessels.[31] Given that hemodynamic forces regulate microvessel remodeling and vessel caliber,[2] the differences in network composition in the framed implants is probably due to structural adaptation stimuli unique to the aligned architecture established by the tissue stress-strain dynamics of uniaxial mechanical loading.

Discussion

The mechanisms underlying the postangiogenesis evolution of microcirculatory architecture are not fully known and are likely varied. We hypothesized that the topology of the final microcirculation is predetermined by the spatial organization of the neovessels giving rise to the new network. We

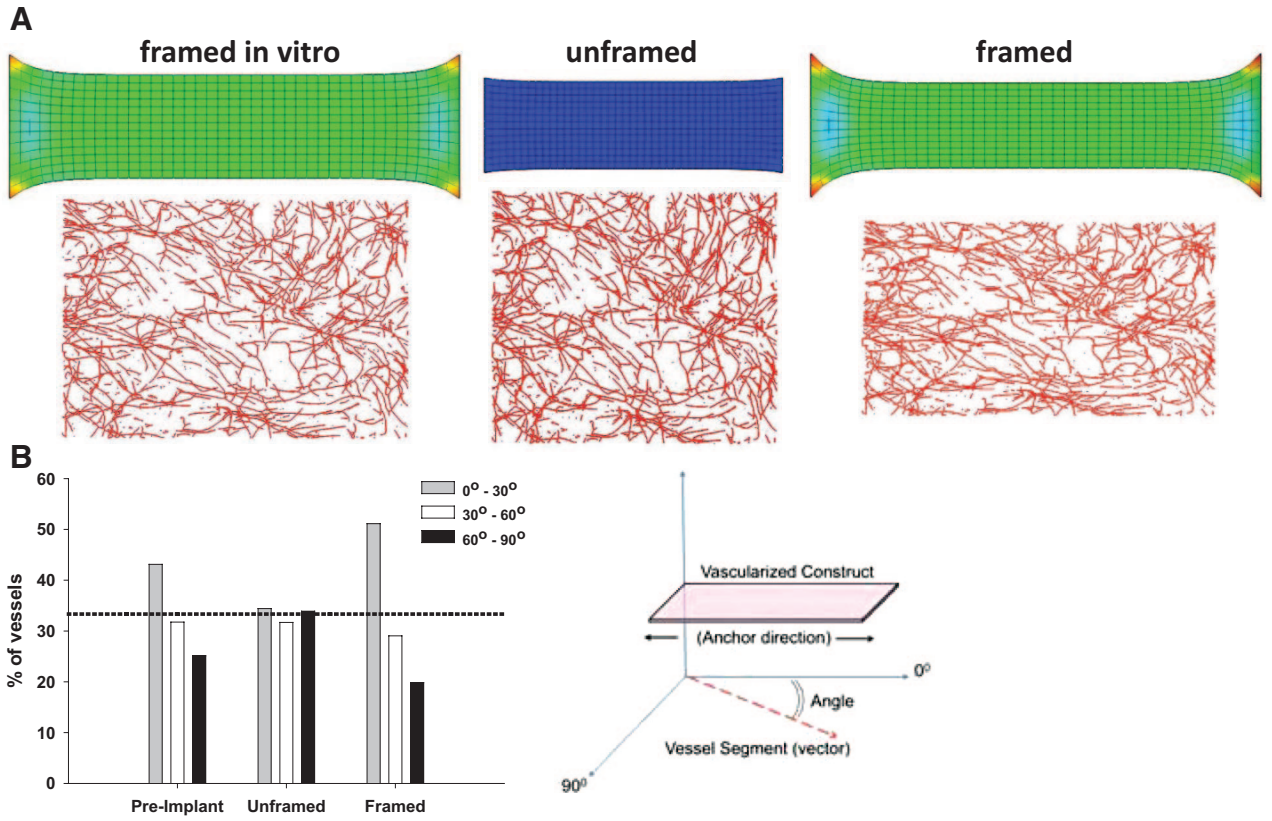

Figure 5. Computer simulations of collagen gel deformation in unframed and framed implants. **A**, Predicted shape-change and strain maps (top row) and microvessel alignments (bottom row) in cultured microvascular constructs (MVCs) (framed in vitro), unframed and framed implants from computer simulations in which the collagen gel was modeled as a compressible neo-Hookean hyperelastic constitutive system with a viscoelastic component. The color scale for the top panel ranges from blue (negative strain, maximum of −0.3 Pa) to red (positive strain, maximum of +0.43 Pa); green represents zero strain. **B**, The percentage of neovessels in each simulated condition in 30° angle bins, where an alignment of 0° indicates an alignment along the direction of constraint according to the schematic shown to the right. The dashed line indicates a system with randomly oriented elements.

reasoned, therefore, that if there was a preexisting neovessel organization in the MVC, then the subsequent network formed following implantation should also be composed of similarly organized microvessels. Our experimental strategy involved prepatterning the isolated microvessel fragments used to form the MVC into unidirectional, parallel arrays during assembly of the MVC followed by an analysis of the form and topology of microcirculatory networks that developed following implantation of the MVCs. We used the MVC as our experimental platform because the neovessels are amenable to manipulation in the initial formation of the construct and they progress to form a mature microcirculation when implanted.[13] In addition, the neovessels are free to remodel and revise as needed during the evolution of the new microcirculation similar to that in native tissues.[4] We used 2 distinctly different strategies for controlling the 3-dimensional orientation of neovessels involving either the direct alignment of neovessels (via bioprinting) or the indirect alignment secondary to physically constraining the MVC (via framing). Both approaches resulted in the parallel alignment of neovessels in the MVC before network progression.

Regardless of the strategy used to prepattern the neovessels, the initial neovascular organization (uniaxial alignment in our case) was lost in the resultant mature network, indicating that prepatterning of angiogenic precursors does not act to determine segment topology in the network during the evolution of the implanted system. The basis of this loss of prepatterning in the implants is not clear from our experiments. However, the low anisotropy index observed after the first week of implantation in the BAT-derived MVCs (Figure 3), a time when blood perfusion begins in the neovasculature of MVCs,[4,13] suggests that the loss of neovessel organization is accompanied by hemodynamics-mediated vascular changes. How vascular responses to hemodynamic inputs would mediate changes in vessel position and orientation is not clear. Certainly, circumferential pressure and shear stress are critical in the diameter adaptation and maturation of microvessels.[8,32–34] However, given the lack of evidence indicating that changes in the spatial 3D positioning of a neovessel and diameter adaptation are coupled, it seems unlikely that adaptation alone is responsible. By applying energy optimization principles, a set of scaling "rules" were developed that dictated the morphological construction of vascular trees.[35] In this mathematical analysis, emphasis was placed on vascular branching, a process inherent in forming tree structures, and overall network scaling. However, it was proposed that circumferential stresses, secondary to hemodynamic forces, were important in establishing the tree structure.[35] Perhaps, then, those hemodynamic forces present in

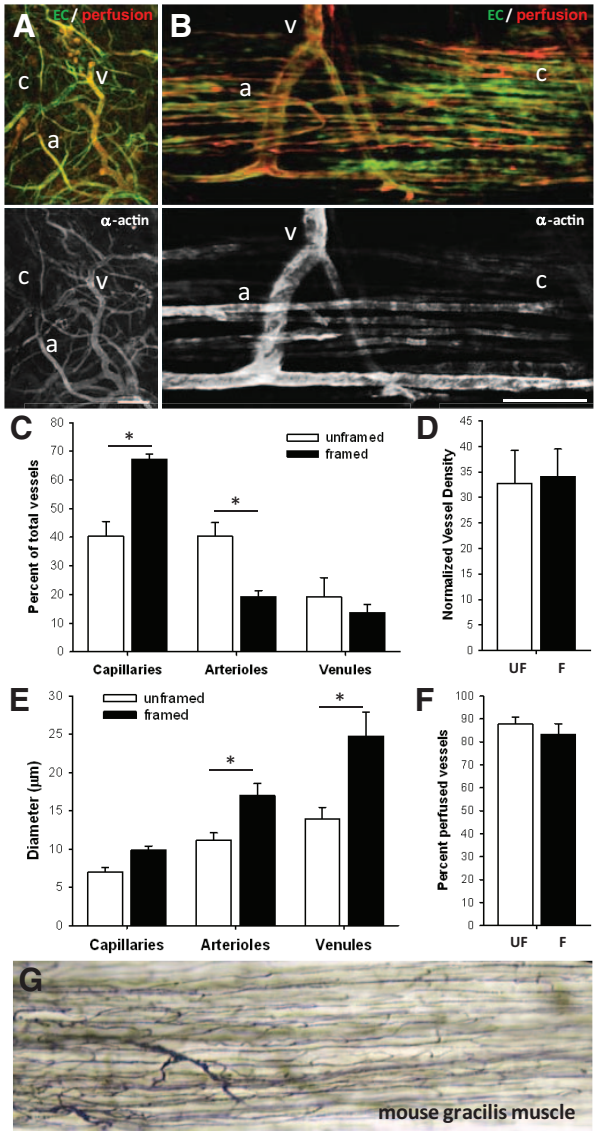

Figure 6. Microvessel composition of mechanically loaded microvascular construct (MVC) implants is different. **A** and **B**, Unframed (**A**) and framed (**B**) implants had microvasculatures that were perfused (top) and are composed of mature arterioles (a), capillaries (c) and venules (v) (bottom). **C**, Networks in framed MVC implants contained proportionally more capillaries and fewer arterioles than those in unframed MVC implants. **D**, Microvascular networks of both unframed (UF) and framed (F) implants had equal numbers of microvessels. **E** and **F**, Arteriole and venule diameters were significantly larger in the framed networks than in the unframed networks and were perfused to an equal extent. **G**, Ink casting of the mouse gracilis muscle vasculature highlighting the similarity between the aligned network in skeletal muscle and the aligned network in the framed MVC implants. Scale bars=200 μm. *$P<0.05$.

the early vasculature promote branching morphogenesis, leading to new segments with new orientations. One can also envision a combination of branching, which places a new vessel segment in a different direction, followed by selective pruning of the downstream parent segment, leaving behind only the newly reoriented new vessel segment. Regardless, our findings suggest that any preexisting neovessel organizational cues are overridden as the network architecture is refined by necessary long-term adjustments in vessel caliber, vessel density, and flow pathway position.

The loss of a preestablished microvessel pattern in the final network architecture occurred in those MVC implants lacking a persistent patterning cue after angiogenesis. Conversely, when a patterning cue (ie, uniaxial framing) was maintained throughout the neovascularization process, microvessel segments in the mature networks were oriented as intended. Thus, although vascular remodeling processes appear not to be profoundly influenced by the initial pattern of neovessels, they are subject to the influences of tissue-derived forces. With the framing experiments and complimentary simulations, we have identified tissue deformation as 1 possible external environmental cue for influencing angioarchitectures. How tissue deformation influenced microvessel positioning within the developing network, even in the presence of active structural adaptation and remodeling, is not clear. Previous and additional new studies (unpublished observations) examining the effects of boundary conditions and mechanical loading of in vitro angiogenesis systems indicate that the viscoelastic properties of collagen gels are such that stresses associated with uniaxial loading are dissipated and likely not significant.[27–29,36] However, although physical stresses are predicted to eventually be minimal in the implants, initially higher stresses and strains are present during the deformation process (primarily in the transverse direction). Whether these transient stress/strain dynamics, alone or in combination with the subsequent deformation cues, influence network topology remains to be determined. Given that there is considerable compression and reorganization of collagen fibrils associated with framed MVCs in culture,[36] this restructuring of the extracellular matrix environment is likely a critical factor in influencing vessel position during tissue deformation. It is reasonable to think that the final shape of a tissue space may be sufficient to influence microvessel orientation within a forming network. However, given our observation that constrained shape (ie, strips) of the MVCs prepared with the BAT bioprinter do not have aligned microvessels following implantation and changing the shape of cultured MVCs in vitro does not affect angiogenic neovessel alignment,[29] it is likely that the final shape itself is not important.

In regenerative therapies, although there remains an emphasis on assembling the individual microvessel precursors (eg, microvessel fragments, vascular cells, and stem cells) that will give rise to the new microvasculature, the importance of constructing a functional network in these therapies is gaining appreciation.[37] Consequently, recent efforts have been exploring strategies for prepatterning these precursors as a means to preform a final, desired network topology.[21,29,38–41] We demonstrate here 2 additional approaches for controlling the organization of vessel elements in 3D space. The framing approach is based on earlier studies showing that uniaxial constrained MVCs lead to the orientation of angiogenic microvessel along the axis of constraint.[29] Others, including ourselves, have used bioprinting, our second approach, to assemble vascular cells into desired network-like patterns or to build large caliber macrovessels.[26,40–43] However, this is the first example of bioprinting

intact microvessel fragments as a prevascularized tissue construct, which raised new technical challenges[26] related to the long aspect ratio of the microvessel elements and collagen matrix. The 2 patterning approaches differ from those involving a lithographic-based approach in which networks of fluidic channels are formed in either hard or soft materials, the walls of which serve as the "walls" of the new vessels once vascular precursors are delivered.[44,45] Unlike with preformed channels, both approaches used here enable manipulation of network precursors while still permitting those vascular activities, such as neovessel remodeling, intrinsic to network formation following implantation. However, despite the success realized in prepatterning the microvessel fragments with these 2 approaches, the pattern was maintained only when a patterning cue was maintained throughout neovascularization. This implies that any regenerative strategy intended to create specific vascular network topologies in vivo should include architectural cues during the postangiogenesis phase, perhaps by controlling the tissue environment as opposed to the vascular elements themselves.

Acknowledgments

We thank Dr Gabriel Gruionu for the image of the ink casting of the mouse gracilis muscle and Shawn Reese for the Fast Fourier transform analysis written for Matlab.

Sources of Funding

This work was supported by National Institutes of Health grants HL077683 (to J.A.W.), DK078175 (to S.K.W.), and EB007556 (to J.B.H.).

Disclosures

None.

References

1. Pittman RN. Oxygen transport and exchange in the microcirculation. *Microcirculation*. 2005;12:59–70.
2. Pries AR, Secomb TW. Control of blood vessel structure: insights from theoretical models. *Am J Physiol Heart Circ Physiol*. 2005;288: H1010–H1015.
3. Hoying JB, Williams SK. Building blood vessels. In: Aird WC, ed. *Endothelial Biomedicine.* Cambridge, United Kingdom: Cambridge University Press; 2007.
4. Nunes SS, Greer KA, Stiening CM, Chen HY, Kidd KR, Schwartz MA, Sullivan CJ, Rekapally H, Hoying JB. Implanted microvessels progress through distinct neovascularization phenotypes. *Microvasc Res*. 2010;79: 10–20.
5. Pries AR, Cornelissen AJ, Sloot AA, Hinkeldey M, Dreher MR, Hopfner M, Dewhirst MW, Secomb TW. Structural adaptation and heterogeneity of normal and tumor microvascular networks. *PLoS Comput Biol*. 2009; 5:e1000394.
6. Pries AR, Reglin B, Secomb TW. Structural adaptation of microvascular networks: functional roles of adaptive responses. *Am J Physiol Heart Circ Physiol*. 2001;281:H1015–H1025.
7. Schaper W. Therapeutic arteriogenesis has arrived. *Circulation*. 2001; 104:1994–1995.
8. Buschmann I, Pries A, Styp-Rekowska B, Hillmeister P, Loufrani L, Henrion D, Shi Y, Duelsner A, Hoefer I, Gatzke N, Wang H, Lehmann K, Ulm L, Ritter Z, Hauff P, Hlushchuk R, Djonov V, van Veen T, le Noble F. Pulsatile shear and Gja5 modulate arterial identity and remodeling events during flow-driven arteriogenesis. *Development*. 2010;137: 2187–2196.
9. Lehoux S, Tronc F, Tedgui A. Mechanisms of blood flow-induced vascular enlargement. *Biorheology*. 2002;39:319–324.
10. Hoying JB, Boswell CA, Williams SK. Angiogenic potential of microvessel fragments established in three-dimensional collagen gels. *In Vitro Cell Dev Biol Anim*. 1996;32:409–419.
11. Gruionu G, Stone AL, Schwartz MA, Hoying JB, Williams SK. Encapsulation of ePTFE in prevascularized collagen leads to peri-implant vascularization with reduced inflammation. *J Biomed Mater Res A*. 2010.
12. Shepherd BR, Hoying JB, Williams SK. Microvascular transplantation after acute myocardial infarction. *Tissue Eng*. 2007;13:2871–2879.
13. Shepherd BR, Chen HY, Smith CM, Gruionu G, Williams SK, Hoying JB. Rapid perfusion and network remodeling in a microvascular construct after implantation. *Arterioscler Thromb Vasc Biol*. 2004;24:898–904.
14. Hiscox AM, Stone AL, Limesand S, Hoying JB, Williams SK. An islet-stabilizing implant constructed using a preformed vasculature. *Tissue Eng Part A*. 2008;14:433–440.
15. Rhoads RP, Johnson RM, Rathbone CR, Liu X, Temm-Grove C, Sheehan SM, Hoying JB, Allen RE. Satellite cell-mediated angiogenesis in vitro coincides with a functional hypoxia-inducible factor pathway. *Am J Physiol Cell Physiol*. 2009;296:C1321–C1328.
16. Nunes SS, Krishnan L, Gerard CS, Dale JR, Maddie MA, Benton RL, Hoying JB. Angiogenic potential of microvessel fragments is independent of the tissue of origin and can be influenced by the cellular composition of the implants. *Microcirculation*. 2010;17:557–567.
17. Chang CC, Nunes SS, Sibole SC, Krishnan L, Williams SK, Weiss JA, Hoying JB. Angiogenesis in a microvascular construct for transplantation depends on the method of chamber circulation. *Tissue Eng Part A*. 2010;16:795–805.
18. Lois C, Hong EJ, Pease S, Brown EJ, Baltimore D. Germline transmission and tissue-specific expression of transgenes delivered by lentiviral vectors. *Science*. 2002;295:868–872.
19. McManus MC, Boland ED, Simpson DG, Barnes CP, Bowlin GL. Electrospun fibrinogen: feasibility as a tissue engineering scaffold in a rat cell culture model. *J Biomed Mater Res A*. 2007;81:299–309.
20. Smith CM, Christian JJ, Warren WL, Williams SK. Characterizing environmental factors that impact the viability of tissue-engineered constructs fabricated by a direct-write bioassembly tool. *Tissue Eng*. 2007;13: 373–383.
21. Smith CM, Stone AL, Parkhill RL, Stewart RL, Simpkins MW, Kachurin AM, Warren WL, Williams SK. Three-dimensional bioassembly tool for generating viable tissue-engineered constructs. *Tissue Eng*. 2004;10: 1566–1576.
22. Sander EA, Barocas VH. Comparison of 2D fiber network orientation measurement methods. *J Biomed Mater Res A*. 2009;88:322–331.
23. Ateshian GA, Rajan V, Chahine NO, Canal CE, Hung CT. Modeling the matrix of articular cartilage using a continuous fiber angular distribution predicts many observed phenomena. *J Biomech Eng*. 2009;131:061003.
24. Matthies H, Strang G. The solution of nonlinear finite element equations. *Int J Numerical Methods Eng*. 1979;14:1613–1626.
25. Bak H, Afoke A, McLeod AJ, Brown R, Shamlou PA, Dunnill P. The impact of rheology of human fibronectin-fibrinogen solutions on fibre extrusion for tissue engineering. *Chem Eng Sci*. 2002;57:913–920.
26. Chang CC, Boland ED, Williams SK, Hoying JB. Direct-write bioprinting three-dimensional biohybrid systems for future regenerative therapies. *J Biomed Mater Res B Appl Biomater*. 2011;98:160–170.
27. Krishnan L, Weiss JA, Wessman MD, Hoying JB. Design and application of a test system for viscoelastic characterization of collagen gels. *Tissue Eng*. 2004;10:241–252.
28. Krishnan L, Hoying JB, Nguyen H, Song H, Weiss JA. Interaction of angiogenic microvessels with the extracellular matrix. *Am J Physiol Heart Circ Physiol*. 2007;293:H3650–H3658.
29. Krishnan L, Underwood CJ, Maas S, Ellis BJ, Kode TC, Hoying JB, Weiss JA. Effect of mechanical boundary conditions on orientation of angiogenic microvessels. *Cardiovasc Res*. 2008;78:324–332.
30. Guilkey JE, Hoying JB, Weiss JA. Computational modeling of multicellular constructs with the material point method. *J Biomech*. 2006;39: 2074–2086.
31. Skalak TC, Schmid-Schonbein GW. The microvasculature in skeletal muscle: IV: a model of the capillary network. *Microvasc Res*. 1986;32: 333–347.
32. Gruionu G, Hoying JB, Pries AR, Secomb TW. Structural remodeling of mouse gracilis artery after chronic alteration in blood supply. *Am J Physiol Heart Circ Physiol*. 2005;288:H2047–H2054.
33. Pries AR, Reglin B, Secomb TW. Remodeling of blood vessels: responses of diameter and wall thickness to hemodynamic and metabolic stimuli. *Hypertension*. 2005;46:725–731.

34. Peirce SM, Skalak TC. Microvascular remodeling: a complex continuum spanning angiogenesis to arteriogenesis. *Microcirculation*. 2003;10: 99–111.
35. Kassab GS. Scaling laws of vascular trees: of form and function. *Am J Physiol Heart Circ Physiol*. 2006;290:H894–H903.
36. Kirkpatrick ND, Andreou S, Hoying JB, Utzinger U. Live imaging of collagen remodeling during angiogenesis. *Am J Physiol Heart Circ Physiol*. 2007;292:H3198–H3206.
37. Lokmic Z, Mitchell GM. Engineering the microcirculation. *Tissue Eng Part B Rev*. 2008;14:87–103.
38. Chang CC, Hoying JB. Directed three-dimensional growth of microvascular cells and isolated microvessel fragments. *Cell Transplantation*. 2006;15:533–540.
39. Norotte C, Marga FS, Niklason LE, Forgacs G. Scaffold-free vascular tissue engineering using bioprinting. *Biomaterials*. 2009;30:5910–5917.
40. Cui X, Boland T. Human microvasculature fabrication using thermal inkjet printing technology. *Biomaterials*. 2009;30:6221–6227.
41. Visconti RP, Kasyanov V, Gentile C, Zhang J, Markwald RR, Mironov V. Towards organ printing: engineering an intra-organ branched vascular tree. *Expert Opin Biol Ther*. 2010;10:409–420.
42. Skardal A, Zhang J, Prestwich GD. Bioprinting vessel-like constructs using hyaluronan hydrogels crosslinked with tetrahedral polyethylene glycol tetracrylates. *Biomaterials*. 2010;31:6173–6181.
43. Khan MS, Fon D, Li X, Tian J, Forsythe J, Garnier G, Shen W. Biosurface engineering through ink jet printing. *Colloids Surf B Biointerfaces*. 2010;75:441–447.
44. Lee W, Lee V, Polio S, Keegan P, Lee JH, Fischer K, Park JK, Yoo SS. On-demand three-dimensional freeform fabrication of multi-layered hydrogel scaffold with fluidic channels. *Biotechnol Bioeng*. 2010;105: 1178–1186.
45. Wang GJ, Ho KH, Hsu SH, Wang KP. Microvessel scaffold with circular microchannels by photoresist melting. *Biomed Microdevices*. 2007;9: 657–663.